Effect of Yttria on the Phase Formation and Sintering of HA-Al$_2$O$_3$ Biocomposites

K.E. Öksüz* and A. Özer

Cumhuriyet University, Department of Metallurgical and Materials Engineering, 58140, Sivas, Turkey

Hydroxyapatite is very-well known as the main component of hard tissues and, as such, it has attracted much attention by researchers in the recent decades. This study was aimed to present the characterization of Y$_2$O$_3$ doped 50 wt.% hydroxyapatite – 50 wt.% Al$_2$O$_3$ composite materials fabricated at relatively high temperature of 1600 °C. Hydroxyapatite powder was obtained from bovine bones via calcination and ball milling technique. Fine powders ($\leq$ 1 μm) of hydroxyapatite/Al$_2$O$_3$ were admixed with 0.5 and 1 wt.% Y$_2$O$_3$ powders. Powder compacts were sintered at 1600 °C for 4 h in air atmosphere. The field emission scanning electron microscopy, energy-dispersive spectroscopy and X-ray diffraction studies following the relative density measurements were conducted. Moreover, the microhardness was studied as the mechanical property of sintered samples. The effect of increasing Y$_2$O$_3$ content on surface morphology, elemental distribution and phase evaluation was investigated in hydroxyapatite/Al$_2$O$_3$ biocomposite materials. It was found that by increasing Y$_2$O$_3$ content, the relative density increased up to 98.8%, while the hardness increased to 863 HV$_{(0.2)}$. The main phases, which were found, are Hibonite – CaO(Al$_2$O$_3$)$_6$ and beta-tricalcium phosphate – Ca$_3$(PO$_4$)$_2$, according to X-ray diffraction pattern.

1. Introduction

Nowadays, more and more bone diseases such as bone infections, bone tumors, and bone loss require bone regeneration. Bone tissue engineering is a complex and dynamic process that initiates with migration and recruitment of osteoprogenitor cells followed by their proliferation, differentiation, matrix formation along with remodeling of the bone [1, 2]. Bone scaffold is typically made of porous biodegradable materials that provide the mechanical support during repair and regeneration of damaged or diseased bone. Researches on bone tissue engineering over the past decades have inspired innovation in novel materials, processing techniques, performance evaluation, and applications. Biocompatible scaffolds with controlled porosity and tailored properties are available today due to innovation in scaffold fabrication using advanced technologies.

Hydroxyapatite (HA, Ca$_{10}$(PO$_4$)$_6$(OH)$_2$) material is very popular for bone restorations since it accelerates the bone growth around the implant due to its chemical and crystallographic similarity to human carbonated apatite [3]. Biomaterials of synthetic HA are highly reliable but the synthesis of HA is often complicated and expensive. Bioceramics of naturally derived biological apatites are more economic. Extensive studies have indicated that HA is biocompatible with hard tissues of human beings and exhibits osteoconductive properties [4–7].

Nevertheless, the mechanical properties of HA are poor, especially in wet environment. Therefore, ceramics of pure HA cannot be suggested for use in heavy-loaded

implants, such as artificial bones or teeth. They can only be used at non-loading applications; such as graft materials.

To improve mechanical reliability of HA-ceramics, i.e. to increase their fracture toughness, incorporation of metallic materials, ceramic oxides [8–10] or fibers can be used. The reinforcement of HA matrices with ceramic particles revealed to have considerable potential for improving the mechanical properties [11]. Among the many ceramics used in orthopedics, alumina (Al$_2$O$_3$) is classified as a bioinert material with excellent friction and wear properties, as well as minimal tissue reaction [12]. In this study, we present the production and characterization of HA-Al$_2$O$_3$ composites, produced via sintering of powder compacts. Bovine derived HA was used and Y$_2$O$_3$-doping was at 0.5 and 1 wt.%. The microstructural observations, phase evaluation, microhardness-density and crystallographic analysis were carried out for the produced samples.

2. Materials and experimental procedure

Bovine femoral bones were cut into small pieces and deproteinized in an alkali solution of 1 wt.% sodium hypochlorite. After washing and drying, the bone pieces were calcined at 850 °C for 4 h in air to totally eliminate any risk of transmitting diseases. The calcined bone pieces were crushed and then ball-milled until fine powders of apatite (BHA $d_{\text{mean}} \leq 1$ μm) was obtained [13–17]. BHA-powders were mixed with 50 wt.% of Al$_2$O$_3$ $d_{\text{mean}} \leq 1$ μm fine powder. In this manner, matrix composition which will be used in the experimental study was prepared.

0.5 and 1 wt.% Y$_2$O$_3$ were correspondingly mixed with HA and Al$_2$O$_3$ powders. These samples are denoted as BHAA, 0.5BHAA and 1BHAA respectively. The powder

———

*corresponding author; e-mail: kerimemreoksuz@gmail.com

mixtures were well homogenized by ball milling in ethyl alcohol using a jar and balls made of zirconia (200 cycles/min, 24 h) with a ball to powder ratio of 20:1. The suspensions were dried and the obtained powders were uniaxially pressed at 350 MPa to form cylindrical pellets with a diameter of 13 mm and height of 10 mm, according to the British Standard [18].

The green bodies were sintered at 1600 °C for 4 h in static air atmosphere in an electric furnace. Micro-hardness tests were done with a Vickers micro-hardness testing equipment (Shimadzu micro-hardness tester type M, Japan; load of 1.961 N; the results were the average of ten different indentation measurements).

The sintered samples were analyzed using field emission gun scanning electron microscope (FEG-SEM, Tescan Mira3 XMU, Czechia) and energy dispersive spectrometer (EDS, AZtec IE, U.K.) for further investigation of grain morphology, shape, size and phase formation. The FE-SEM samples were examined by secondary electron detector at an accelerating voltage of 15–20 kV. EDS was used to determine their surface composition in a ≈ 0.01 mm^2 area, at source energy of 10 keV. X-ray Diffractometer (Rigaku D/MAX/2200/PC) with a monochromatic Cu-K$_\alpha$ radiation ($\lambda = 1.5408$ Å) with an accelerating voltage of 40 kV and a current of 40 mA was used over a 2θ range from 20° to 80° to characterize the crystal structure of the sintered samples.

3. Results and discussion

3.1. Fabrication of raw powders

Figure 1 represents the FE-SEM image of initial powders after ball milling for 24 h. As illustrated in Fig. 1a the powders have relatively narrow particle size distribution without yttria addition. This could be attributed to the very hard and brittle nature of bovine bone and aluminum oxide.
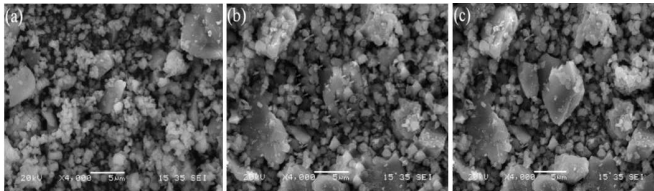

Fig. 1. FE-SEM image of initial powders after ball milling for 24 h. (a) BHAA, (b) 0.5BHAA, (c) 1BHAA. †HA was derived from freshly-extracted bovine femoral bones. Al$_2$O$_3$ and Y$_2$O$_3$ are commercial.

Figure 1b and c shows the existence of yttria by increasing weight percent. By increasing yttria content the powders, especially Al$_2$O$_3$ are in the tendency of formation of Al-Y and Ca-P-Y related phases which are more ductile than bovine bone and aluminum oxide. This is also evident from wide particle size distribution.

3.2. Phase evaluation

The X-ray diffraction patterns of the bioceramic composites sintered at 1600 °C for 4 h are summarized in

Fig. 2. Two crystalline phases, namely Hibonite – CaO (Al$_2$O$_3$)$_6$ and beta-tricalcium phosphate – Ca$_3$(PO$_4$)$_2$, with varying peak intensities, can be detected in the patterns. In all cases, the diffractograms have predominantly registered the Hibonite phase – CaO(Al$_2$O$_3$)$_6$, matched in every sample (ICSD card no. 76-0665), which is due to the dissolution of CaO from HA and its reaction with Al$_2$O$_3$ which makes 50 wt.% in the composite (see Fig. 2a–c).

X-ray diffraction patterns of HA-Al$_2$O$_3$ composite powders show that the peaks correspond to HA and Al$_2$O$_3$ phases, confirming that Al$_2$O$_3$ is effectively incorporated into the HA matrix by forming hibonite. Another registered major phase was beta-tricalcium phosphate. Increasing crystallinity (increase of the peak intensities) in Fig. 2c is attributed to the formation of Ca-Al related phases, accompanying tricalcium phosphate, as previously indicated in Fig. 2a and b. CaY$_2$O$_3$ could not be detected in the XRD patterns after sintering, as a pure substance, suggesting that Y^{3+} ions are dissolved in the HA lattice and sat at interstitial positions, as expected, because of the size difference of their ionic radii [19].
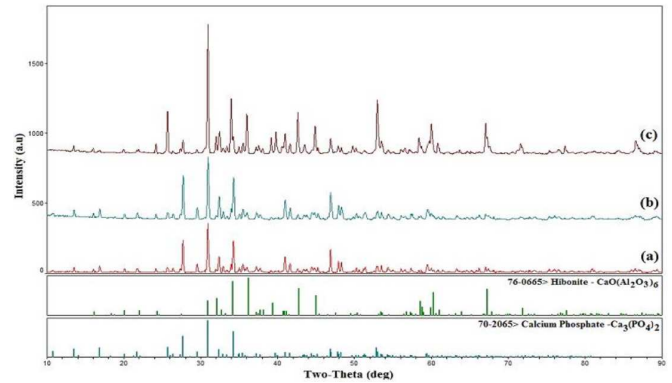

Fig. 2. XRD patterns of biocomposite samples produced with various amounts of Y$_2$O$_3$, after sintering at temperature of 1600 °C for 4 h. (a) BHAA, (b) 0.5BHAA, (c) 1BHAA.

3.3. SEM and EDS analyses

The surface morphology of the BHAA-Y$_2$O$_3$ biocomposites was examined by FE-SEM (SEI) equipped with an EDS. The EDS spectra were observed with an image analyzing program. As seen from Fig. 3a and b, the matrix phase underwent a solid state reaction with a little amount of inter-layer liquid phase coming from the formation of hibonite phase, which is a binary solid compound of CaO-Al$_2$O$_3$, with higher alumina content. The sintering surface observed in Fig. 3a, seems to show uncompleted solid reaction with smooth and growing regions.

Figure 3c and d illustrates the 0.5 Y$_2$O$_3$ added BHAA. The surface becomes smoother with small grains that complete the spreading glassy phase and even forming some grown single phase hexagonal structures of Al-Y phases, leading to the existence of new phases in XRD

pattern. Since the amount of Al-Y and Ca-Y-P related phases is less than 2–3 vol.%, the XRD pattern cannot show the corresponding phases.

Figure 3e and f shows the 1 wt.% Y_2O_3 added BHAA, sintered at 1600 °C. The surface becomes smoother with increasing amount of Y_2O_3 by liquid phase formation at high temperature. The increasing Y_2O_3 content increases the glassy phase and also the hexagonal shaped hibonite and other related phases to a much extent. The surface was coated with a thin layer of Ca-Al-P liquid phase, which acts as a seed liquid for the formation of other single crystal of dissolved elements. The thermodynamic stability of elements at elevated temperature specifies the formation as the Ca-Y-Al-P deficient phases and the Al-Y phases, as can be concluded from the 2θ peak at 26.1°.

Fig. 4. The EDS spectra of the surfaces of (a) BHAA, (b) 0.5BHAA, (c) 1BHAA biocomposites sintered at 1600 °C for 4 h.
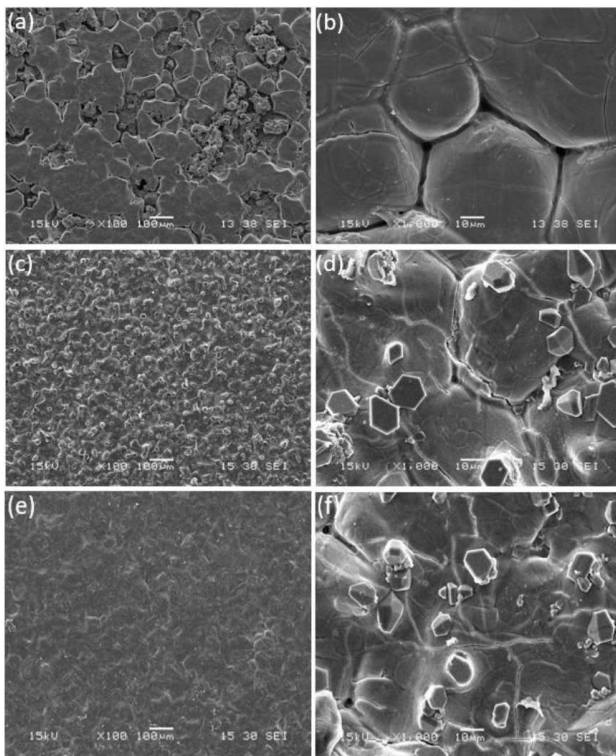

Fig. 3. FE-SEM images of the BHAA-Y_2O_3 biocomposites sintered at 1600 °C for 4 h. (a, b) BHAA, (c, d) 0.5BHAA, (e, f) 1BHAA.

The EDS analysis, as seen from Fig. 4a–c, was carried out for regions from the images in Figure 3b, d and f, respectively. The increasing amount of Y increases the liquid phase and also the dissolution and spreading of Y, as seen from EDS analysis. The inset tables represent the elemental weight ratios of sintered biocomposites with the increasing amount of Y.

3.4. Micro-hardness and relative density of composites

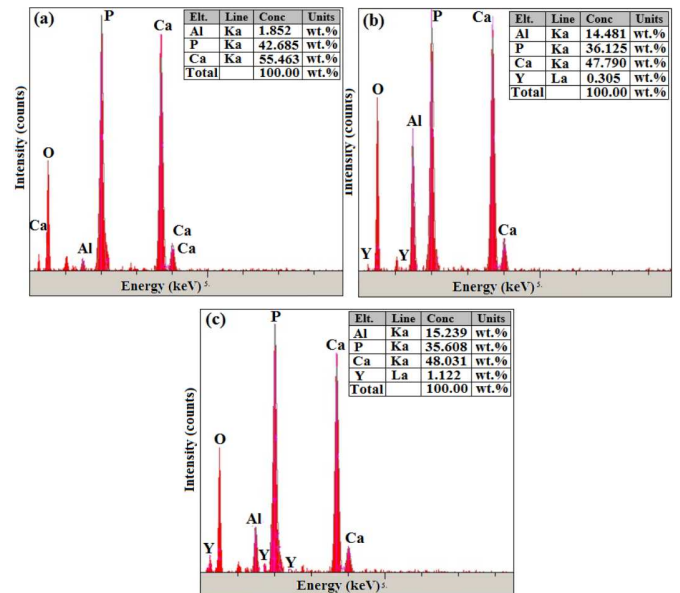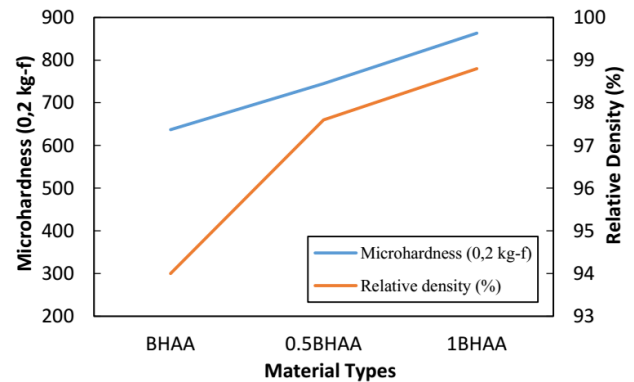The impact of yttria on BHAA matrix was evident in the micro-hardness analysis results. The obtained

Fig. 5. Variations in relative density and micro-hardness of HA/Al_2O_3 composites with different Y_2O_3 contents.

micro-hardness values are considerably higher than those of the BHAA matrix samples. Hardness of composites increased considerably with the introduction and with the increase of the Y_2O_3 addition from 0.5 wt.% to 1 wt.%. These have increased from 637 ± 18.45 HV, to 745 ± 14.1 HV and 863 ± 8.6 HV for the BHAA matrix, 0.5BHAA and 1BHAA samples, respectively. This might be due to finer Y_2O_3 particles and achievement of enough bonding between BHAA matrix, accompanied with the increasing glassy phase amount. The increasing amount of Y_2O_3 also leads to the appearance of new phases, as mentioned before for the liquid phase formation, as seen in Fig. 3b, d and f. The grain boundaries got smoother by increasing Y amount, which may be attributed to Al-Y and Ca-Y-P phases existing between the matrix grains [10]. By glassy phase formation, the amount of interfering obstacles of grains decrease and sudden grain growth at relatively high temperature of 1600 °C,

which gives rise to relative density from 94%±0.7 to 98.8%±0.55, is observed. Variations in relative density and micro-hardness in HA/Al$_2$O$_3$ composites with different Y$_2$O$_3$ contents are shown in Fig. 5.

4. Conclusions

The composites with equal weight ratios of the powders of HA (derived from bovine bone) and Al$_2$O$_3$, with varying concentrations of Y$_2$O$_3$, were produced using a conventional powder metallurgy route and sintered successfully at 1600 °C for 4 h. The increasing Y$_2$O$_3$ amount increased the glassy phase formation, as was evident from both, the FE-SEM and XRD evaluation. The hardness of samples with increasing Y$_2$O$_3$ amounts had increased by increasing glassy phase formation, which leads to the existence of Ca-Y-Al-P related phases. The relative density of samples increased from 94% to 98.8% of theoretical density, with the homogeneous distribution of glassy phase and more smooth surface, resistant to cracking. The reproducible microhardness, phase analyses and morphological evaluation suggest that these materials would have good performance in load bearing applications.

References

[1] P.V. Giannoudis, H. Dinopoulos, E. Tsiridis, *Injury* **36**, 20 (2005).

[2] X. Li, L. Wang, Y. Fan, Q. Feng, F.Z. Cui, F. Watari, *J. Biomed. Mater. Res.* **101**, 2424 (2013).

[3] J.H.G. Rocha, A.F. Lemos, S. Agathopoulos, P. Valèrio, S. Kannan, F.N. Oktar, J.M.F. Ferreira, *Bone* **37**, 850 (2005).

[4] M. Jarcho, *Clin. Orthop. Relat. Res.* **157**, 259 (1981).

[5] K. De Groot, C.P.A Klein, J.G.C Wolke, J.M.A. De Blieck-Hogervorst, *Handbook of bioactive ceramics*, vol. 2, CRC Press, Boca Raton 1990.

[6] L. Hong, H.C. Xu, K. De Groot, *J. Biomed. Mater. Res.* **26**, 7 (1992).

[7] J.T. Edwards, J.B. Brunski, H.W. Higuchi, *J. Biomed. Mater. Res.* **36**, 454 (1997).

[8] G. Goller, F.N. Oktar, *Mater. Lett.* **56**, 142 (2002).

[9] Z.E. Erkmen, Y. Genc, F.N. Oktar, *J. Am. Ceram. Soc.* **90**, 2885 (2007).

[10] K.E. Öksüz, A. Özer, *Dig. J. Nanomater. Biostruct.* **11**, 167 (2016).

[11] L.L. Hench, E.C. Ethridge, *Biomaterials: An interfacial Approach*, Academic Press, New York 1982, p. 384.

[12] B. Masson, R. Rack, G. Willmann, H.G. Pfaff, *Biomech. Biomater. Ortop.* **14**, 143 (2004).

[13] A.F. Lemos, J.M.F. Ferreira, *Key Eng. Mater.* **254–256**, 1037 (2004).

[14] F.N Oktar, M. Yetmez, S. Agathopoulos, G. Lopez, G. Goller, I. Peker, J.M.F. Ferreira, *J. Mater. Sci: Mater. Med.* **17**, 1161 (2006).

[15] J. Chevalier, *Biomater.* **27**, 535 (2006).

[16] J. Chevalier, S. Deville, E. Munch, R. Jullian, *Biomater.* **25**, 5539 (2004).

[17] A.B. Khalil, S.W. Kim, Y.K. Kim, *Mater. Sci. Eng. A* **456**, 368 (2007).

[18] *British Standard Non-metallic materials for surgical implants*, Part 2, *Specification for ceramic materials based on alumina*, BS (No 7253), Part 2, ISO 6474-1981 (1990).

[19] C. Vasconcelos, *Sintering of Ceramics — New Emerging Techniques*, Publisher-Intech, 2012.